Quantitative Analysis of the Cr-depleted Layer in the Heat Affected Zone of Low Carbon Martensitic Stainless Steel†

NAKAMICHI Haruo[*1] NORO Hisato[*2] MIYATA Yukio[*3]

Abstract:

Intergranular stress corrosion cracking (IGSCC) has been observed in the heat affected zone (HAZ) of low carbon martensitic stainless steel. In this study, the authors assessed Cr-depleted zones at the grain boundaries by a STEM-EDX analysis and determined the morphology by deconvolution of the STEM-EDX results. Findings of the authors indicate that Cr-depleted zones of only a few nanometers in width are sufficient to cause IGSCC at the HAZ of low carbon martensitic stainless steel under certain circumstances.

1. Introduction

Low carbon martensitic stainless steels with carbon concentrations of about 0.01 mass % are highly reliable for industrial use and have been used as line pipes since the late 1990's[1,2]. Intergranular stress corrosion cracking (IGSCC) was previously observed in the heat affected zone (HAZ) of this material[3]. This was unexpected, given that IGSCC is fully suppressed at the HAZ in a similar low carbon level SUS304 steel. This new type of IGSCC has also been observed under a particular stress corrosion test condition[4,5]. The factors dominating this IGSCC at the HAZ in low carbon martensitic stainless steel remain unclear and will have to be fully elucidated before this steel can be safely used. Based on the current knowledge of SUS304, the Cr-depleted zones are presumed to be one of the factors responsible for this fracture[5,6]. In several experiments, Cr-depleted points were detected just at the grain boundary[5,6]. These results alone, however, are too incomplete to reliably evaluate the Cr-depleted zone morphologies, such as the width and depleted Cr value. The Cr concentration of low-C martensitic steel (11 mass% Cr) is much lower than that of austenite stainless steel (18 mass% Cr). The diffusion constant of Cr in martensitic steel is much higher than that in austenite steel, and the solubility product of Cr carbides in martensitic steel is much lower than that in austenite steel. These properties pose difficulties in evaluating a Cr-depleted zone, because the zone is smaller and narrower in martensitic steel. An accurate investigation of nano level Cr-depleted zone morphologies is therefore important and necessary for our understanding of the fracture mechanism of this material.

Field-emission TEM (FE-TEM) is one of the most powerful tools for evaluating nano-scale structures. In the present work the authors applied systematic STEM-EDX analyses to detect and evaluate the Cr depletion zone morphology and to acquire knowledge of the factors contributing to IGSCC in low carbon martensitic steels.

2. Experimental Procedure

Low carbon martensitic stainless steels for seamless line pipe of the composition shown in **Table 1** were used in the present experiments. Before stress corrosion testing, the samples were subjected to two-step heat treatment cycles in a Gleeble tester to sensitize them for

† Originally published in *Corrosion Science* Vol. 50, No. 2 (2008), p. 309–315

[*1] Dr. Eng.,
Senior Researcher Manager,
Analysis & characterization Res. Dept.,
Steel Res. Lab.,
JFE Steel

[*2] Ph.D.,
Senior Researcher Deputy General Manager,
Analysis & characterization Res. Dept.,
Steel Res. Lab.,
JFE Steel

[*3] Senior Researcher Manager,
Tubular Products & Casting Res. Dept.,
Steel Res. Lab.,
JFE Steel

Table 1 Chemical composition of the low carbon martensitic stainless steel used in the present paper

(mass%)

Fe	C	Si	Mn	P	S	Cr	Ni
Balance	0.013	0.15	1.1	0.017	0.002 7	11.1	1.5

SCC. The samples were heated at 1 300°C for 1 s (1st step), cooled to room temperature, heated at 650°C for 1 s (2nd step), then cooled to room temperature in a jet of argon gas. This two-step treatment was carried out to simulate the HAZ heat history of the condition imposed during the girth welding of a seamless line pipe.

Scanning election microscopy (SEM) observations were performed on SCC test specimens. Stress was applied by bending the specimens into a U shape. The samples were held in a corrosive environment consisting of 5% NaCl aqueous solution at pH2.5, with 1 bar CO_2 at 70°C for 168 hours. Cracks were observed in the specimens after they were put through two heat cycles of 1 300°C for 1 s and 650°C for 1 s. SEM samples were prepared by electro-polishing at room temperature in a 10% perchloric methanol electrolyte. SEM observation was carried out using FE-SEM (LEO-1530, Carl Zeiss NTS GmbH.) with an accelerated voltage of 3 kV.

The specimens used for the TEM observations to evaluate the Cr-depleted zone morphologies after the sensitized heat treatment condition were not subjected to SCC tests beforehand. A 3 mm diameter disk TEM sample was prepared by twin-jet electro-polishing at −25°C and 30 V, with the same electrolyte used for the SEM samples. The TEM observation was carried out using an FE-TEM (CM-20FEG, FEI Comp.) equipped with EDX (Phoenix, EDAX, Inc.) and an electron energy loss spectroscopy (EELS) system (GIF, Gatan Inc.). STEM-EDX line analyses were performed using a drift correcting program. The specimen thickness and electron beam diameter were measured by an EELS technique and by direct recording of TEM films, respectively.

3. Results and Discussion

3.1. Crack and Grain Boundary Morphologies

Photo 1 shows SEM photographs for a specimen after SCC tests. The crack has propagated along the large angle grain boundary (prior austenite boundary), and a row of small precipitates (white contrast) is formed along the grain boundary nearby. **Photo 2** shows TEM bright field micrographs of a specimen after the second heat treatment. Small precipitates are also dispersed along the prior austenite grain boundary in the TEM image. The carbides were found to be the $M_{23}C_6$ type with an atomic ratio of approximately Cr:Fe=7:3.

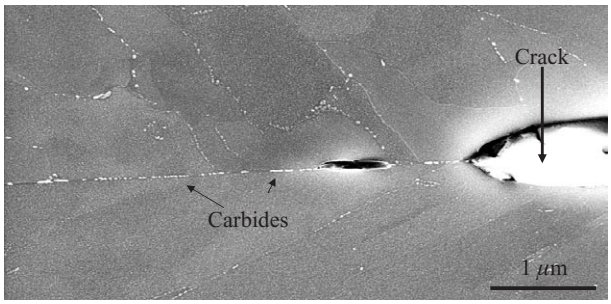

Photo 1 SEM micrograph of the crack morphology after the SCC test (Small white dot contrast corresponds to small carbides.)

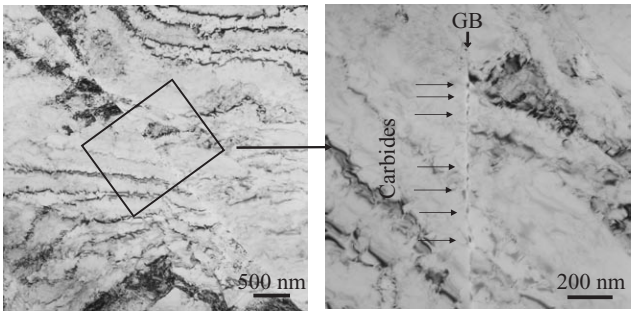

Photo 2 TEM micrographs of the prior austenite grain boundary (Micrographs are taken with a defocused bright field technique and small carbides are identified as black dots within the image.)

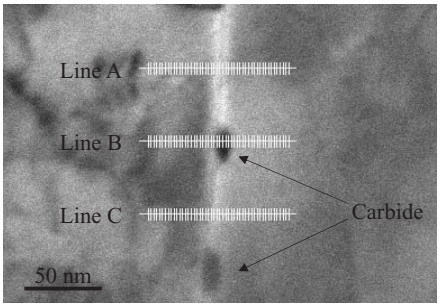

Photo 3 A STEM bright field image of a prior austenite grain boundary (Lines for EDX spectrum analysis are shown on the figure.)

Photo 3 shows a STEM bright field image at a prior austenite grain boundary. The lines in the photo were generated by EDX spectrum mapping performed across this prior austenite grain boundary. Each line has 50 points with a 1.9 nm step, and the acquisition time for EDX analysis was 15 live-seconds. For precise evaluation of the element distribution on the boundary, EDX analysis was performed by tilting a grain boundary perpendicularly to the EDX detector window and electron beam. For the drift compensation program applied after each point acquisition, the spatial error of each analytical point was less than 1 nm. All EDX spectra are stored in the analysis (spectrum mapping).

3.2 Cr Profile of STEM-EDX Analysis

Figure 1 shows typical EDX spectra of the matrix and the grain boundary. Cr and Fe peaks are clearly

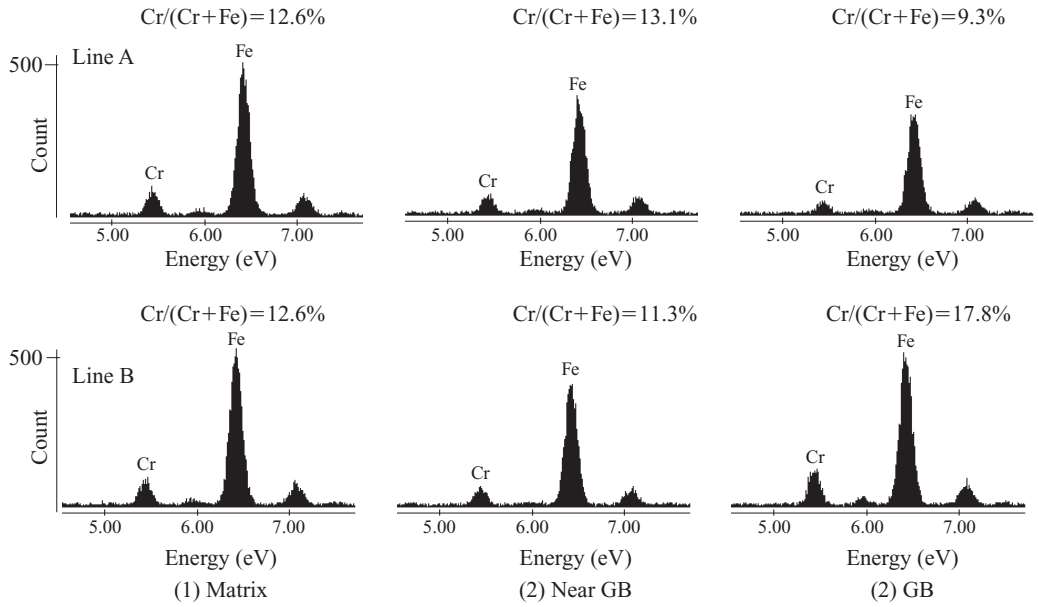

Fig. 1 Typical EDX spectra of the line analysis across the grain boundary (Here measured Cr concentration values, which are calculated by the thin film model using Fe and Cr binary elements, are shown together with the spectrum.)

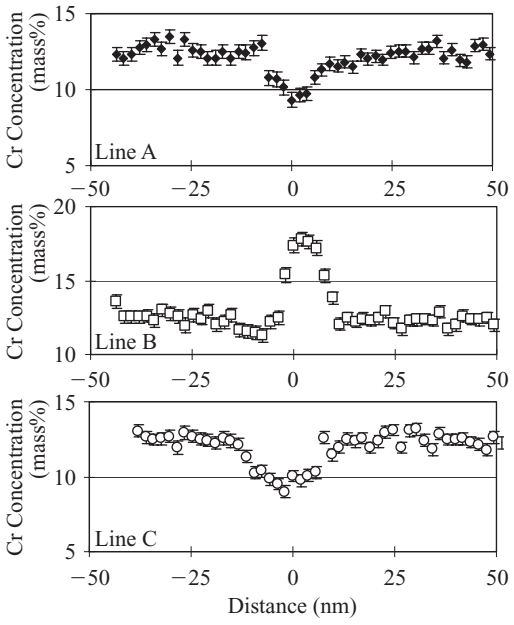

Fig. 2 Cr distribution across the prior austenite grain boundary (Cr depleted zones are identified along line A and C.)

recognized and both elements appear to have enough intensity for quantitative analysis. Several peaks for minor elements, such as Ni or Si, can also be observed. The Fe and Cr distribution is calculated based on an Fe and Cr binary element method using a thin film calculation model[7] to avoid the effect of small elements. The figure also shows the Cr concentration (mass%) calculated for each spectrum. **Figure 2**, meanwhile, shows the measured Cr distribution across the prior austenite grain boundary with statistical error bars ($\pm 1\sigma$). Cr depleted zones are clearly observed along lines A and C.

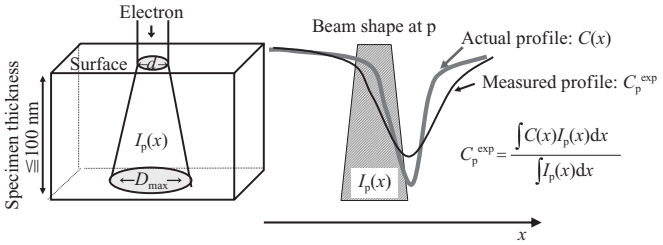

Fig. 3 Schematic model of electron beam spreading in TEM specimens (The measured and actual Cr distribution profiles in a TEM specimen are also shown.)

3.3. Quantitative Estimation of the Cr Depleted Zone

The depleted zone morphologies were investigated by deconvoluting the profile shown in Fig. 2. The scattering of the electron beam in the specimens widens the distribution of the measured EDX analysis peak profiles and pushes up the minimum value, as compared with the actual distributions. **Figure 3** shows a schematic diagram of the spreading electron beam shape ($I_p(x)$), measured profile (C_p^{exp}) at the point of p, and the actual Cr distribution ($C(x)$) in the specimen.

The EDX analysis yields a measured concentration value at p (C_p^{exp}), i.e., at the average value of the actual distribution in the beam volume $I_p(x)$ as described in Eq. (1):

$$C_p^{exp} = \frac{\int C(x)I_p(x)dx}{\int I_p(x)dx} \quad \cdots\cdots (1)$$

The beam spreading shape and specimen thickness are both taken into account in the calculation of the actual distribution morphology. According to ref. 8), the beam diameter at the bottom of the samples is defined as,

$$D_{\max} = (b^2 + d^2)^{\frac{1}{2}} \quad \cdots\cdots (2)$$

where d is an incident beam diameter at the top surface of the specimen and b is defined by,

$$b = 7.21 \times 10^6 \frac{Z}{E}\left[\frac{\rho}{A}\right]^{\frac{1}{2}} t^{\frac{3}{2}} \quad \cdots\cdots (3)$$

where Z is the atomic number of the sample, ρ is the density of the sample (g/cm^3), t is the specimen thickness (cm), E is the energy of incident electron (eV), and A is the mass number of the sample.

The specimen thickness is estimated using an EELS method[9]. **Figure 4** shows an EEL spectrum at the STEM-EDX spectrum mapping area (Photo 3). The thickness of the specimen is defined by the following Eq. (4):

$$\frac{t}{\lambda} = \ln\left[\frac{I_e}{I_i}\right] \quad \cdots\cdots (4)$$

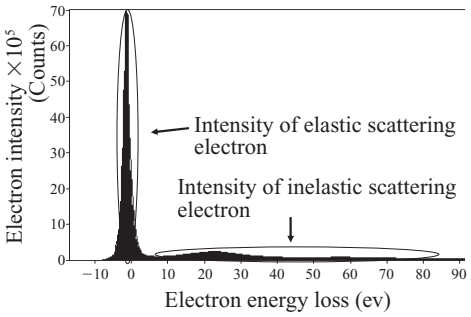

Fig. 4 EEL spectrum from the STEM-EDX analysis area (In the present experiment, the $\ln(I_e/I_i)$ value is 0.54.)

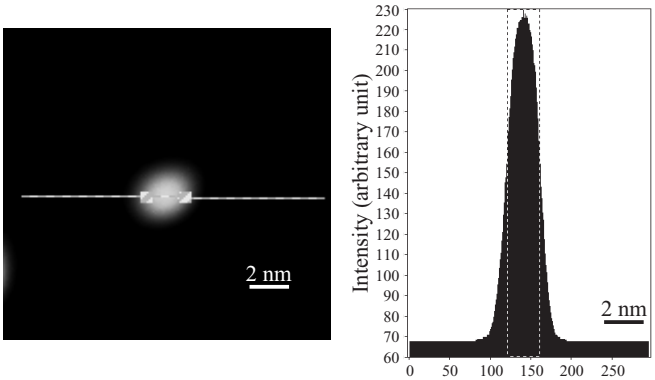

Fig. 5 Photograph and intensity profile of the incident electron beam (The beam diameter is estimated to be 2.1 nm at FWHM.)

I_e and I_i are the intensities of elastic and inelastic scattered electrons, respectively, t is the specimen thickness, and λ is the mean free path of electrons, i.e., 74 nm in Fe for 200 kV electrons. In this experiment, $\ln(I_e / I_i)$ is 0.581 and the specimen thickness is calculated to be 43 nm. **Figure 5** shows the incident beam shape and intensity profile. The diameter of the incident electron beam (d) is estimated to be 2.1 nm at FWHM. By substituting the specimen thickness and incident beam diameter values into Eqs. (2) to (4), the authors calculate a value of 3.8 nm for $D_{\max}$ and define the beam shape as ($I_p(x)$).

Gaussian and linear function distributions were used to evaluate the distributions of Cr ($C(x)$) in the present paper. The formula and parameters are shown in **Table 2**. Parameter fitting is carried out by a least mean square approximation using measured distribution results from lines A and C in Fig. 5, and the results for the fitting parameters of deconvolution are shown in **Table 3**. Deconvoluted distribution curves of lines A and C are shown in **Fig. 6**. Table 3 also shows the Cr depletion value (ΔC) and depleted zone width (w), the latter of which is determined from the FWHT of the depleted Cr profile. The results of this analysis suggest a Cr depleted zone morphology of 10 to 15 nm in width and around a 9 mass% for the minimum Cr. This tiny width and the amount of Cr depletion morphology are deduced to be sufficient to cause IGSCC under the particular circumstance condition in ref[10], that is, conditions which simulate the HAZ conditions of the seamless pipe girth welding.

4. Conclusion

Cracks propagate along prior austenite grain boundaries where rows of carbides have formed and where the

Table 2 Assumed functions and parameters for the Cr distribution

	Gaussian	Linear
Function	$C(x)=12.5-C_0\exp\left(-\frac{x^2}{\sigma^2}\right)$	$C(x)=\pm\alpha x+b$ $\left\{-\frac{(12.5-b)}{a}\leqq x\leqq\frac{(12.5-b)}{a}\right\}$
Parameters	C_0, σ	a, b

Table 3 Definition of Cr distribution parameters. Values of Cr depletion (ΔC) and depleted zone width (w) are also shown in this table

	Gaussian				Linear			
Results	C_0	σ	ΔC (mass%)	w (nm)	a	b	ΔC (mass%)	w (nm)
Line A	3.3	6.7	3.3	11.4	0.40	8.7	3.8	8.2
Line C	3.5	9.3	3.5	15.2	0.36	8.2	4.3	11.8

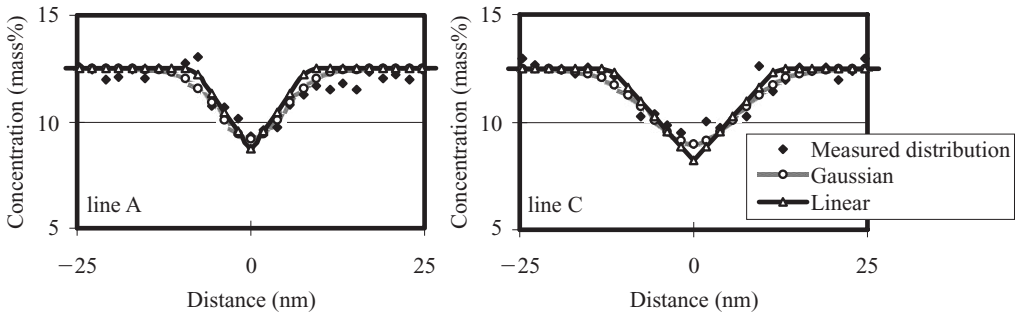

Fig. 6 Deconvoluted Cr profiles for lines A and C (in Fig.2) (Cr distributions are estimated based on two distribution functions. A summary of the distribution morphologies is shown in Table 3.)

Cr-depleted zone across the prior austenite grain boundaries is detected precisely by STEM-EDX mapping. The Cr-depleted zone morphologies reveal that the minimum Cr concentrations within the depleted zones are about 75% of the matrix Cr concentration, with depleted zone widths between 10 and 15 nm. Depleted zones this narrow are sufficient to instigate IGSCC in super martensitic stainless steels.

Specimen preparation procedures were performed by JFE Techno-Research.

References

1) Ueda, M.; Amaya, H.; Kondo, K.; Ogawa, K.; Mori, T. Corrosion96. 1996, paper no. 58.
2) Miyata, M.; Kimura, M.; Murase, F. Kawasaki Steel Technical Report. 1998, no. 38, p. 53.
3) Van Gestel, W. Corrosion2004. 2005, paper no. 04141.
4) Rogne, T.; Svenning, M. Supermartensitic Stainless Steels 2002. 2002, no. P028.
5) Gregori, A.; Woollin, P.; van Gestel, W. Eurocorr2004. 2004, 13-0-433.
6) Ladanova, E.; Solberg, J. K.; Rogne, T. Stainless Steel World. 2003-12. p. 17.
7) Cliff, G.; Lorimer, G. W. Journal of Microscopy. 1975, vol. 103, p. 203.
8) Reed, S. J. B. Ultramicroscopy. 1982, vol. 7, p. 405.
9) Egerton, R. F. Electron Energy-Loss Spectroscopy in the Electron Microscope. 2nd Ed., New York, Plenum Press, 1996.
10) Miyata, Y.; Kimura, M.; Nakamichi, H.; Sato, K.; Itakura, N.; Masamura, K. Corrosion2005. 2005, paper no. 05095.